"Redox processes on ceria and a Rh/CeO2 catalyst followed by X-Ray absorption in the fast acquisition mode"

ARTICLE *in* THE JOURNAL OF PHYSICAL CHEMISTRY B · JANUARY 1994

Impact Factor: 3.3

7 AUTHORS, INCLUDING:

Jaafar El Fallah

Université de Caen Normandie

42 PUBLICATIONS **1,192** CITATIONS

SEE PROFILE

A. Kiennemann

University of Strasbourg

248 PUBLICATIONS **6,211** CITATIONS

SEE PROFILE

Francois Le Normand

University of Strasbourg

205 PUBLICATIONS **2,432** CITATIONS

SEE PROFILE

Redox Processes on Pure Ceria and on Rh/CeO_2 Catalyst Monitored by X-ray Absorption (Fast Acquisition Mode)

J. El Fallah,[†,‡] S. Boujana,[§] H. Dexpert,[∥] A. Kiennemann,[§] J. Majerus,[†] O. Touret,[⊥] F. Villain,[∥] and F. Le Normand*[,†,#]

Laboratoire de Catalyse et de Chimie des Surfaces, UA 423 du CNRS, Institut Le Bel, Université Louis Pasteur, 67070 Strasbourg Cedex, France, Laboratoire pour l'Utilisation du Rayonnement Electromagnétique (LURE), Centre Universitaire Paris-Sud, 91405 Orsay Cedex, France, Laboratoire de Chimie Organique Appliquée, UA 469 du CNRS, EHICS, 1, rue Blaise Pascal, 67037 Strasbourg Cedex, France, and Centre de Recherches Rhone-Poulenc, 52, rue de la Haie Coq, 93308 Aubervilliers Cedex, France

Received: December 28, 1993[⊗]

Redox processes occurring on ceria and Rh on ceria catalyst have been monitored by X-ray absorption spectroscopy (XAS) at the Ce L_{III} edge using a fast collection mode of the data. From changes in the Ce L_{III} shape, a quantitative evaluation of the Ce(III)/Ce(IV) content has been monitored within an error estimated to 5%. This kinetic study is both confirmed and extended to N_2O chemisorption and thermogravimetric measurements. The influence of the ceria surface area and the effect of rhodium are investigated in detail. The redox processes are simulated by alternate exposure to H_2 and dry air at atmospheric pressure and moderate temperatures (573–773 K). The initial reduction content is dependent on the ceria surface area, and a kinetic model accounting for this behavior is developed. Between 573 and 673 K the reduction starts on the surface through successive hydrogen dissociation and anionic vacancy formation, followed by a much slower bulk diffusion step. It is stated that the hydrogen dissociation is the limiting step of the surface process on pure ceria. On Rh/CeO_2 sample the surface reduction becomes very fast, due to the faster hydrogen dissociation on metallic rhodium. By contrast with reduction, the kinetic behavior for oxidation is very fast on pure ceria, but needs an induction time on Rh/CeO_2. These deep differences for the redox properties induced both by the high surface area of ceria and the presence of a transition metal are related to the behavior of ceria for depollution catalysis.

I. Introduction

The use of ceria as a promoter in catalysis for automotive pollution control could be partially related to its unique ability to store or remove oxygen in the course of the depollution process.[1,2] Catalysts consist typically of ceria and a transition metal (Pt, Pd, or Rh) supported on alumina. The reducibility of ceria is enhanced by the presence of a transition metal. This effect is now well supported by thermoprogrammed reduction (TPR), X-ray photoemission (XPS), and X-ray photoabsorption (XAS) measurements.[2-5] This behavior contrasts with the difficulty of reducing pure ceria in the conditions of depollution ($T > 573$ K). In addition, some difficulties still subsist on ascertaining if the substoichiometric phases $CeO_{(2-x)}$ then formed are well or badly ordered.[6] On the other hand, data on the kinetic processes of reduction and oxidation are rather scarce.[7-10] Moreover, the samples concerned by these studies were generally calcined at high temperatures, so that they exhibited a low surface area. However, in a recent publication, an easier reducibility for a high surface area sample was reported, an effect which emphasizes the role played by the surface in the reduction process.[7] To monitor the change of the cerium oxidation state during a fast reduction process, X-ray absorption on the Ce L_{III} edge was recorded in the fast acquisition mode.[11] In that way, it is a complementary probe to XPS, which gives mainly information on the surface,[4,5,12-14] or extended X-ray absorption spectroscopy (EXAFS), which provides information on the structural modifications related to the change of the oxidation state.[15] The aim of this paper is then to gain further insight into the kinetics of the reduction and oxidation processes on the time scale of a few seconds. We focused in a first approach on the H_2 reduction and air reoxidation as probes of the reductive and oxidative behavior, respectively.

The samples we studied include pure ceria, of low and high surface areas, and ceria as support of a transition metal (Rh) catalyst.

The layout of the paper is as follows. After the introduction (part I), the experimental basis of the study (part II) is described. In part III the assignation of the Ce L_{III} absorption edge features is briefly discussed. Then a method for a quantitative shape analysis of the Ce L_{III} edge is derived, which allows the extraction of the Ce(III)/Ce(IV) content. Kinetic results on both the reduction and the oxidation processes obtained within a time scale of about 1000 s are then displayed (part IV). Thermogravimetric analysis (TGA) and N_2O chemisorption experiments complement these results. They are included for two reasons. This is first another way to check the validity of the quantitative interpretation extracted from XAS. Secondly, the X-ray beam provided by Synchrotron Radiation can be used only for reasonable time-consuming experiments, and there was a need to extend our set of data to a longer time scale (1–30 h), particularly for slow kinetics. The result is that a kinetic model can then more reliably be proposed in the Appendix and checked. The effects of both the ceria surface area and the occurrence of a transition metal on the reduction–reoxidation behavior are finally discussed in the framework of this heterogeneous kinetic model (part V). The main conclusions are recalled in part VI.

II. Experimental Section

(1) Samples. The main properties of the samples used in the present study are given in Table 1. Samples A_1 and A_2 were provided by Rhone-Poulenc Recherches (calcined in air 6 h at

* To whom any enquiries should be addressed.
† Laboratoire de Catalyse et de Chimie des Surfaces.
‡ Present address: Laboratoire de Catalyse et de Spectrochimie, UA 414 du CNRS, ISMRa, 6, Boulevard du Maréchal Juin, 14050 Caen Cedex, France.
§ Laboratoire de Chimie Organique Appliquée.
∥ Centre Universitaire Paris-Sud.
⊥ Centre de Recherches Rhone-Poulenc.
Present address: Institut de Physique et Chimie des Matériaux, Groupe Surfaces-Interfaces (IPCMS-GSI), UMR 46 du CNRS, Bat. 69, 23, rue du Loess, 67037 Strasbourg Cedex, France.
⊗ Abstract published in *Advance ACS Abstracts*, April 15, 1994.

0022-3654/94/2098-5522$04.50/0

TABLE 1: Main Characteristics of the Samples

sample	no.	air treatment (°C)	S_{BET} (m^2/g)	weight (%) metal	Cl
CeO_2 RP	A_1	400	125		
CeO_2 RP	A_2	850	8		
CeO_2 JM	A_3		≤5		
Rh/CeO_2	B	400	110	1.45	1.16

673 and 1123 K, respectively). The surface areas determined by BET were 125 and 8 m^2/g, respectively. The CeO_2 purity was 99.5%, with La_2O_3 as the main impurity (0.3%). Sample A_1 presented a high proportion of microporous area.[16] Sample A_3 was provided by Johnson–Matthey (minimum purity 99.99%).

Rh/CeO_2 (1.45%) was obtained by dry impregnation of sample A_1 with the appropriate content of $RhCl_3$ solution. The catalyst was then dried overnight at 393 K, calcined 1 h in dry air at 673 K, and finally sieved at 20 μm. The samples were stored in a desiccator before any further use.

HRTEM examination of the catalyst reduced at 673 K indicated that the rhodium particles have a mean size of 2–3 nm.[17]

(2) TGA. Thermogravimetric experiments under a reductive atmosphere were carried out in a Setaram microbalance connected to a high-vacuum device. A sample of ca. 70 mg was first calcined 1 h at 673 K under dry air, cooled down, and evacuated (down to 10^{-6} Torr) at room temperature. The sample was then exposed to a hydrogen flow (150 mL/min at atmospheric pressure) and isothermally reduced by steps of 50 K, from 298 K to the ultimate reduction temperature. Hydrogen was preliminarily purified through a palladium membrane. We consider that equilibrium was reached when the weight variation per hour was lower than 0.1% of the overall weight change. Typically, more than 20 h of isothermal exposure to hydrogen were required at low temperatures to fulfill this condition.

(3) XAS. Ce L_{III} edge absorption experiments were recorded on the EXAFS III station of the DCI storage ring (LURE, Orsay). Two parallel Si(311) crystals were used as monochromator. One of them was tilted so that most of the harmonics were rejected. The X-rays beam slits were adjusted to a final resolution of about 3 eV at the cerium $Ce(OH)_3$ or $Ce(NO_3)_3$ edge. Two Keithley proportional chambers filled with an appropriate gas under static pressure measured the incident (I_0) and the transmitted (I) beams. X-ray energies were calibrated to the copper edge at 8991.1 eV. The single Ce L_{III} absorption edge peaked then at 5725 ± 1 eV. The data acquisition used the fast acquisition setup, which was previously described.[11] In our conditions, data were collected in an energy range of 100 eV around the Ce L_{III} edge in 12 s with a good signal to noise ratio.

Samples were preliminarily sieved to 10 μm and ultrasonically dispersed in an ethanol solution. Some drops were withdrawn from this dispersion and slowly spread on a graphite Papyex sheet. After evaporation of the solvent, a second graphite sheet was pressed on it, forming the reaction cell. The cell was then mounted in a stainless steel block provided with gas circulation (30 mL/min) and temperature control. Graphite sheets were pressed so that the controlled pressure drop between the gas inlet and outlet of the cell never exceeded 5% of the atmospheric pressure. We checked that under these conditions no preferential pathways existed for the gas circulation throughout the sample in the course of the kinetic experiments. Other aspects of this cell were described in more detail in the literature.[18] The amount of solid dispersion was adjusted so as to obtain a penetration depth by the X-rays of around 10–20 μm, corresponding to the optimum absorption $\log(I/I_0) = 1.5$–2.5, using the absorption coefficients given by the MacMaster tables.[19] Under these conditions we can estimate that the X-ray beam crossed about five to ten layers of ceria particles. As the absorption edge step for a single layer is less than 0.1, negligible distortion occurred in the absorption edge due to a leakage effect.[20]

Prior to the kinetics experiments, the samples were calcined 1 h in situ under dry air. After the sample reached the required working temperature, gas composition was changed by rapidly switching the gas inlet. The beginning of the kinetics ($t = 0$) was arbitrarily referenced to the first detection of a shape modification of the Ce L_{III} edge (Figure 4). Dry air and H_2 (purity 99.995%) from L'Air Liquide were used without further purification. Unless otherwise stated, the gas flows were 30 and 15 mL/min for H_2 and air, respectively.

(4) N_2O Reactivity. N_2O adsorption experiments were performed at 593 K in a volumetric apparatus already described.[21] Reoxidation of ceria (ca. 500 mg) by N_2O occurred through chemical reaction I:

$$CeO_{(2-x)} + xN_2O \rightarrow CeO_2 + xN_2 \qquad (I)$$

Pulses of N_2O in helium were injected, and the outgoing gas was chromatographically analyzed. Injections were stopped if both of the following conditions were fulfilled: (i) the N_2 peak disappeared and (ii) the N_2O peak was saturated. The total volume V_{N2O} required for the complete reoxidation of ceria was then given by formula 1:

$$V_{N2O} = V_B \sum_i ((A_s - A_i)/A_s) \qquad (1)$$

where V_B is the volume of the gas loop, A_s and A_i are the surface areas of the N_2O peak at the saturation and the injection i, respectively. We checked that the N_2O consumption was equal to the N_2 evolution within 5%.

Attempts to measure the ceria reduction content by N_2O adsorption on the Rh/CeO_2 catalyst were unsuccessful as O_2 was also evolved from the outgoing gas.

H_2 (purity 99.999%) and dry air from L'Air Liquide were used without further purification.

III. Ce(III) and Ce(IV) Oxidation States Deduced from the XAS Analysis of the L_{III} Edge

(1) Ce L_{III} Edge. In order to obtain quantitative information from the analysis of the Ce L_{III} edge, we must first recall experimental and theoretical assignments of the L_{III} cerium absorption edge given in the literature.

The Ce L_{III} absorption edge of a pure Ce(IV) compound such as CeO_2 exhibits three distinct lines, denoted A, B_2, and C, respectively (Figure 1), in good agreement with previous reported spectra of CeO_2.[22] With enough resolution, a structure B_1 appears clearly as a shoulder of the most intense B_2 structure. These lines were not only observed on other Ce(IV) compounds such as $Ce(SO_4)_2$[23] or CeF_4[24] but also on other rare earth oxides with the fluorite structure (PrO_2, TbO_2),[25] although their intensities and relative energy positions were slightly modified according to the nature of the material. Their occurrence was related to the symmetry of the local environment around the absorbant cation Ce(IV). Kotani et al.[26] were the first to point out a charge transfer from valence O 2p states to Ce 4f localized states of the rare earth in the final state. This charge transfer was responsible for the multiple contributions observed in the Ce L_{III} edge, as for the Ce 3d core level photoemission features.[27] Inverse photoemission investigations[28] and valence band calculations[29] supported the conclusion that this charge transfer was rendered possibly by the strong f character of some valence band O 2p states. This assumption could then reconcile the XAS and XPS spectroscopic investigations with the macroscopic properties of CeO_2, which is well-known to be an insulator and a diamagnetic phase. This also means that the Ce–O bond has a partially covalent character.[30]

Whereas most authors agreed to assign the wide line C to the Ce $[2p^54f^05d^*,^1]$ O $2p^6$ final state configuration (possibly with some weak contribution of the Ce $[2p^54f^25d^*,^1]$ O $2p^4$ final state[27]), some controversy still persists when assigning the B_1 and B_2 lines.

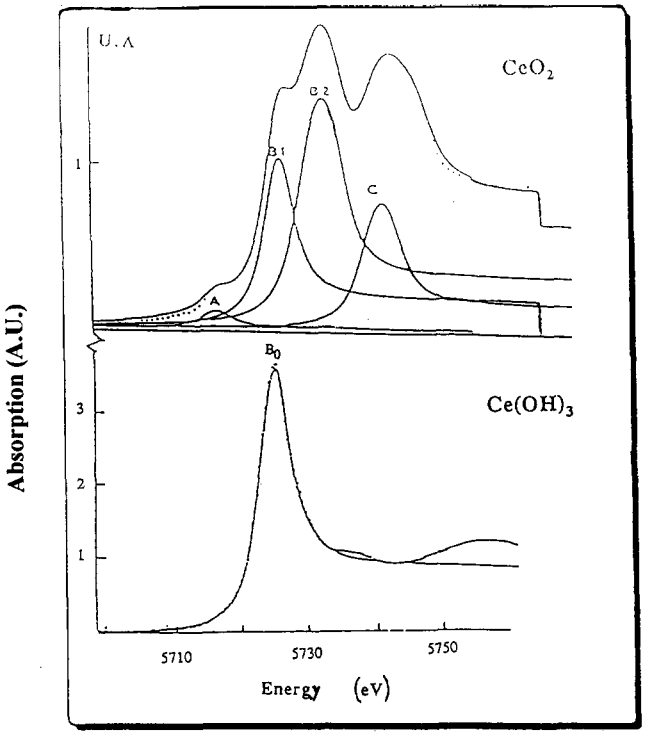

Figure 1. Ce L_{III} edge of CeO_2 and $Ce(OH)_3$, reproduced by the courtesy of E. Beaurepaire et al.[22b].

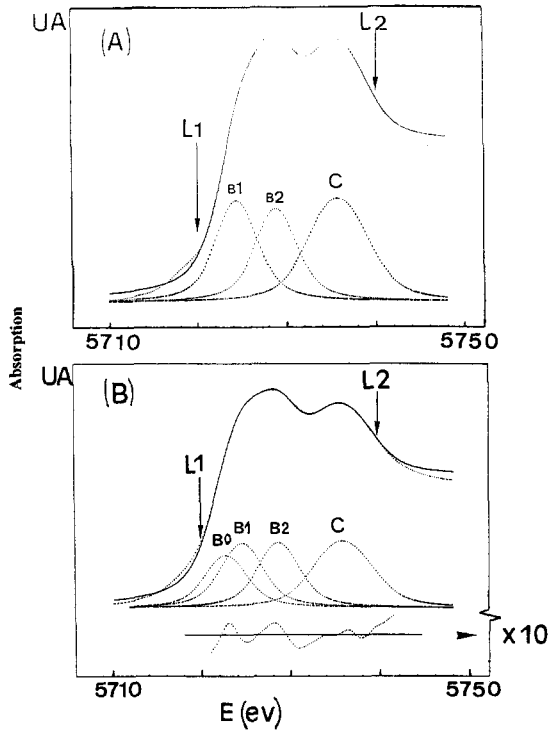

Figure 2. Fit of CeO_2 (A) and reduced CeO_2 (B). L1 and L2 represent the low and high limits of the fitting domain, respectively. The difference spectrum is displayed below part B on a 10-fold scale. See the text for the assignment of the various features.

Bianconi[23] and Kotani[27] assigned these lines to a strong mixture of Ce $[2p^54f^15d^*,^1]$ O $2p^5$ and Ce $[2p^54f^25d^*,^1]$ O $2p^4$ states, respectively. The additional introduction of a coulombic repulsion term between the f and d electrons in the final state contributes however to a sharp decrease, if not a disappearance of the Ce $[2p^54f^25d^*,^1]$ O $2p^4$ contribution. Kaindl[24] assigned the B_1 structure to Ce(III) impurities. This suggestion seems however unlikely, as we found that the B_1 feature still persists on CeO_2 in an oxidative environment where the presence of Ce(III)

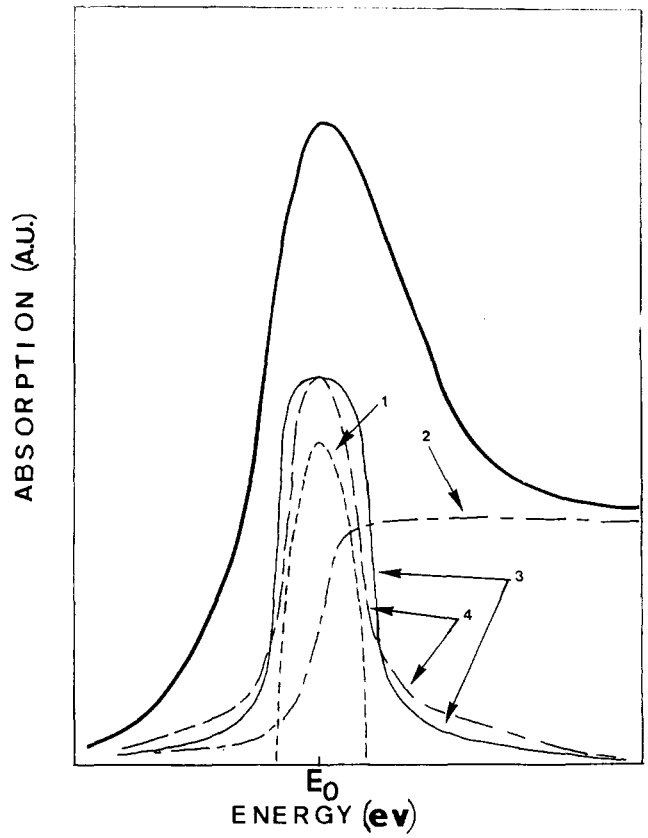

Figure 3. Analysis procedure of the Ce L_{III} edge. The calculated overall contribution (thick line) is obtained by the convolution of (1) a density of empty states; (3) an experimental resolution; (4) the core hole lifetime to which is added (2) the transitions toward the continuum states. The analytical form of each of these contributions is detailed in the text.

impurities is highly improbable. Dexpert et al.[25] introduced localized (B_1) and delocalized (B_2) 4f final states, in relation to the reported nature of the valence band. Finally, the very weak feature A can be attributed (i) to transitions toward Ce 6s states allowed by the dipole selection rule or (ii) to the presence of impurities (hydroxyl groups, etc.). This very weak contribution will be neglected in the following.

By comparison, the shape of the Ce(III) absorption state is quite simple, as only one single line noted B_0 in Figure 1 is observed. This white line was assigned to the Ce $[2p^54f^15d^*,^1]$ O $2p^6$ final state, the 4f states being strongly localized well behind the valence states in the Ce(III) ground configuration. This single line was observed whatever the nature of the Ce(III) compound: $Ce(OH)_3$,[22b] $Ce(NO_3)_3$,[23] or CeF_3.[24] We determined an energy difference of 1.85 eV between this line and the B_1 line of CeO_2 (Table 2), both by recording the two reference compounds CeO_2 and $Ce(OH)_3$ successively and from the best fit agreement obtained on a partially reduced ceria (Figure 2). The B_0 line pointed at a lower energy than any other features of the CeO_2 edge.

In conclusion, the Ce L_{III} absorption edge provides well-characteristic fingerprints of the Ce(IV) and Ce(III) oxidation states, respectively. The Ce(IV) oxidation state yields the characteristic lines A (neglected), B_1 and B_2 (hardly separated), and C, whereas the Ce(III) oxidation state yields the single line B_0 hardly separated from the B_1 and B_2 features. Thus, only a line-shape analysis could provide the relative contribution of each oxidation state in a mixed situation.

(2) Quantitative Analysis. The fitting procedure used a computer program slightly modified by comparison with the fits reported in ref 7 (Figure 3). The background was first removed and the spectra were normalized to the absorption of the continuum states. This was achieved by reference to the inflexion points of

TABLE 2: Parameters Used in the Fitting Procedure of the Ce L_{III} Absorption Edge.[a]

	BE (eV)				W (eV)			
sample	B_0	B_1	B_2	C	B_0	B_1	B_2	C
A_1	0	1.85	5.65	12.25	3	3	3	8.6–9.6
A_2	0	1.85	5.65	12.25	3	3	3	8.6–9.6
A_3	0	1.85	5.65	12.25	3	3	3	8.6–9.6
B	0	1.85	5.95	13.0	3	3	3	8.0–9.0

[a] Binding energies (BE) were referenced to the Ce(III) B_0 line. Other parameters were G = 3.0 eV; Γ = 3.16 eV.

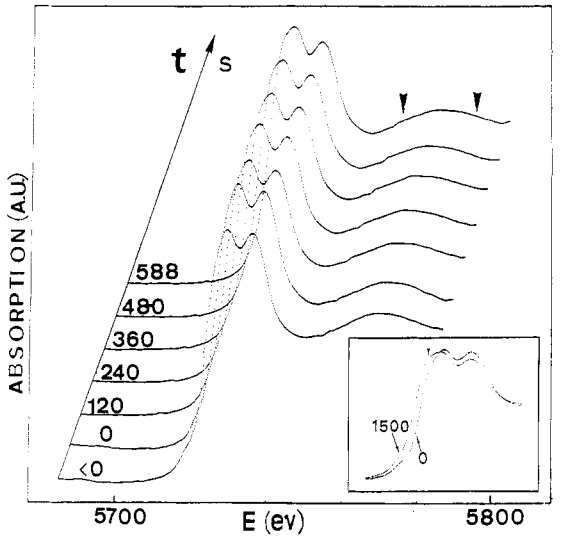

Figure 4. Cd L_{III} edge evolution with time during the reduction of the sample A_1 at 673 K. The beginning of the reduction is arbitrarily defined at the time where the shape line begins to change. The arrows indicate the normalization points by reference to the inflexion points of the near absorption edge structure. In the inset we present the initial spectrum and the spectrum recorded after 1500 s of hydrogen exposure.

the intense near absorption edge structure that occur at around 20 eV above the threshold (Figure 4). Each line was then adjusted by a convolution of the following contributions (Figure 3 and Table 2):

(1) The lifetime of the 2p hole was simulated by a Lorentzian line shape with a Γ width of 3.16 eV.[31]

(2) The experimental resolution was adjusted by a Gaussian line shape with a G width of 3 eV.

(3) The density of unoccupied 5d states was fitted by a parabolic function with a W width reported in Table 2. This contribution to the broadening of the peak was fixed to 3 eV, except for the high-energy contribution where the width was much larger (around 9 eV).

These different contributions were then convoluted and added to the transitions toward the continuum states simulated by a step function convoluted with the experimental and core hole lifetime broadenings.

The thresholds of the step functions were taken at the B_0 and B_1 energies with intensities proportional to the Ce(III) and the Ce(IV) absorption intensities, respectively.

Experimental spectra were fitted by a Simplex method, in which only the intensity of each line and the broadening W of the line C were allowed to vary. For a given sample, the relative binding energies were kept constant. A small energy shift was however observed between samples A and B. A similar behavior was reported on CeO_2–TiO_2 mixed oxides.[32] This small energy shift can be attributed to a crystal field effect in the fluorite structure. In addition, the difference spectrum between the experimental and calculated spectra is also reported in Figure 2b. It was checked that the error was randomly distributed on the overall energy range of the fit. The energy domain where the calculation is

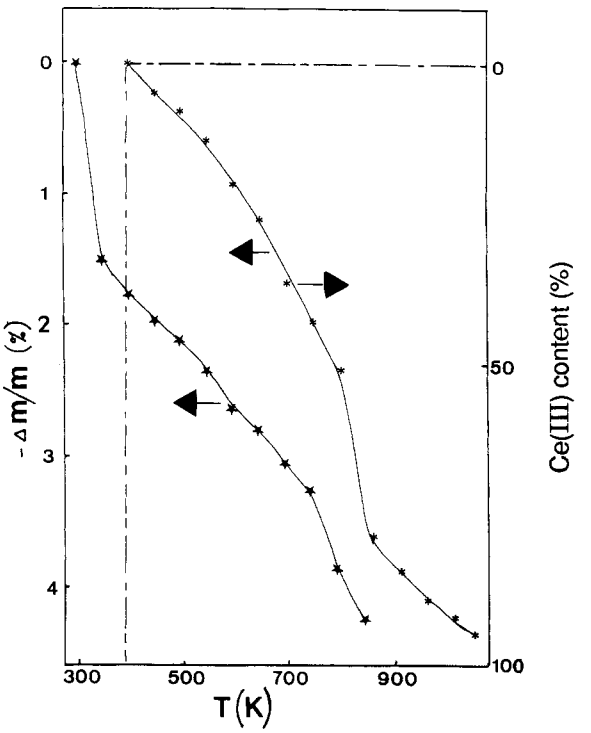

Figure 5. Thermogravimetric analysis on ceria samples: asterisk, sample A_1; star, B; left ordinate, weight loss $-\Delta M/M$ (%); right ordinate, Ce(III) reduction content on sample A_1 deduced from the chemical reduction II.

performed (L1–L2 domain on Figure 2, which represents around 20 eV) was restricted at high energy so as to minimize the multiple-scattering effects which started to occur in this energy range.

The determination of the reduction content was estimated from the relative area of the B_0 contribution, compared to the sum of the areas of each contribution, according to

$$\text{Ce(III)} = B_0/(B_0 + B_1 + B_2 + C) \quad (2)$$

and the reduction content $\alpha(t)$ was defined as

$$\alpha(t) = \text{Ce(III)}/(\text{Ce(III)} + \text{Ce(IV)}) \quad (3)$$

The error in the Ce(III) content determination was estimated to 5%.

IV. Results

(1) Thermogravimetric Results. The weight variation $-\Delta M/M$ (%) with the reduction temperature up to 1043 K for sample A_1 and 823 K for sample B, respectively, is displayed in Figure 5. A continuous weight loss was obtained. The process was however accelerated between 743 and 843 K for both samples. Between 298 and 393 K, some weight loss was observed on sample A_1 that we assigned to the evolution of adsorbed water. At temperatures higher than 393 K, the weight loss was attributed to the reduction of ceria according to global equation II:

$$2CeO_2 + H_2 \rightarrow Ce_2O_3 + H_2O \quad (II)$$

The reduced amount deduced from the weight loss above 393 K according to eq II is reported on the left ordinate of Figure 5. Within this assumption, the ceria was almost fully reduced at 1043 K.

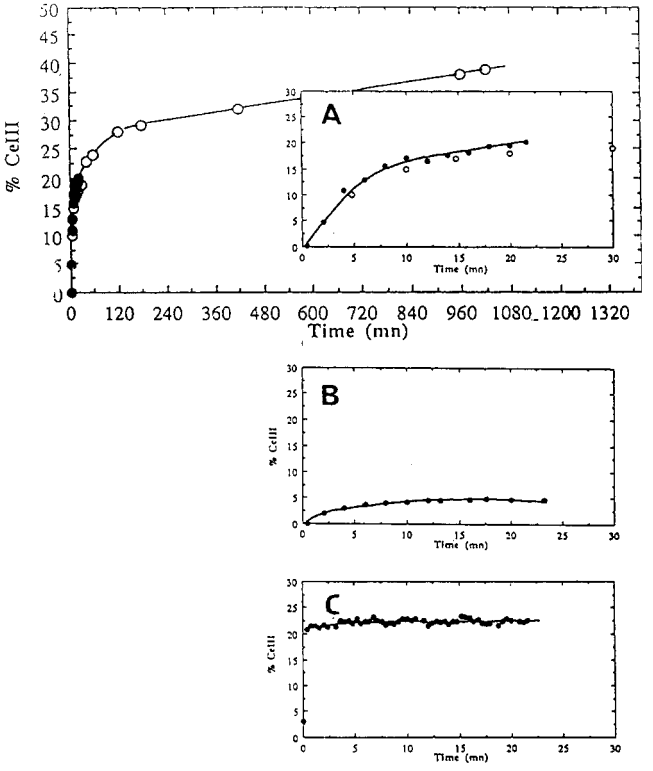

Figure 6. Reduction kinetics on (A) CeO_2 sample A_1; (B) CeO_2 sample A_2; and (C) Rh/CeO_2 sample B at 673, 753, and 673 K, respectively: filled circles, XAS of the Ce L_{III} edge; empty circles, N_2O adsorption.

On the Rh/CeO_2 sample, the process was more complex, as we also had to include the reduction of Rh particles according to

$$Rh_2O_3 + 3H_2 \rightarrow 2Rh^0 + 3H_2O \qquad \text{(III)}$$

and the hydrogen chemisorption and desorption equilibrium on the metallic rhodium,

$$Rh^0 + (x/2)H_2 \rightleftarrows RhH_x \qquad \text{(IV)}$$

As reported by XPS,[33] the reduction of ceria in the presence of rhodium occurred even at room temperature. We thus reported the weight loss between 302 and 402 K that we assigned both to rhodium oxide and ceria reduction.[34] We noted that the slope of $-\Delta M/M$ above 402 K is lower than on pure ceria, with a sharp decrease above 743 K. Nevertheless, the weight difference at 843 K between the two samples (0.54%) cannot be fully accounted for by the reduction of rhodium according to eq III (1.13%). As the rhodium is fully reduced and the equilibrium IV is displaced toward hydrogen desorption at high temperatures, this difference meant that the ceria is less reduced in the presence of rhodium.

(2) XAS. *(a) Reduction.* The evolution of the Ce L_{III} edge with time is plotted for sample A_1 in Figure 4. Qualitatively, the reduction process resulted in an increase in the contribution noted B_0 and in a decrease of the other contributions. This is clearly apparent in the inset of Figure 4 when superposing the normalized initial ($t = 0$) and the reduced ($t = 1500$ s) spectra. The time scale was referenced to the moment when line-shape modifications began to occur. In Figure 6 (insets) the kinetics of reduction content, determined by the curve-fitting procedure and eqs 2 and 3, are plotted for CeO_2 A_1 and A_2 and Rh/CeO_2 at 673, 753, and 673 K, respectively. The temperature domain investigated ranged between 573 and 773 K.

Large modifications of the Ce L_{III} edge line shape initially occurred on pure ceria sample A_1. The process then slowed down,

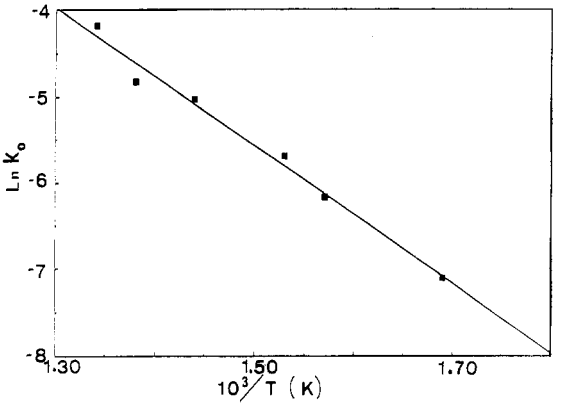

Figure 7. Arrhenius plot $\ln k_0 = f(1/T)$: sample A_1, ΔT = 573 –773 K.

but variations of the L_{III} edge line shape were still detectable, even after a long time of hydrogen exposure.

Above 673 K for sample A_1, we always observed some discontinuity during the reduction process (not shown). After a sharp initial increase of the B_0 intensity (about 1 min), discontinuous behavior was observed. Moreover, the mean degree of reduction $\alpha(t)$ defined by eq 3 generally decreased. For example, the Ce(III) content after 25 min of reduction was 20, 16, and 8% at 673, 723, and 753 K, respectively. As we will discuss later, this effect can be attributed to pore filling, which occurs in addition to some chemical reduction. BET measurements performed on the same sample A_1 clearly indicated that the surface area sharply decreased under hydrogen above 673 K.[16] The surface was not stabilized above 673 K. This physical process competing with the reduction process precluded us from further studying the reduction above 673 K. However, assuming that this pore filling was in fact a direct consequence of the reduction process, its initial rate was negligible. Thus, the experimental rate constant of the initial reduction k_0 represented the rate constant of the virgin sample. k_0 values were extracted from the initial slope of the curve % Ce(III) = $f(t)$ (Figure 6). The report of k_0 in an Arrhenius plot (Figure 7) within the temperature range 573–773 K led to an activation energy of 67 ± 12 kJ/mol.

The low surface area sample A_2 exhibited a much weaker reduction (around 4%), which occurred at temperatures highly than 753 K only (Figure 6B). Sample A_3, which is of a different origin, behaved quite similarly to sample A_2.

Finally, we performed repeated isothermal cycles of reduction–reoxidation, and we obtained quite reproducible degrees of reduction, provided the reduction temperature did not exceed 673 K. In separate experiments, N_2 was admitted for 0.5 h between air and H_2. No detectable change was observed due to this additional treatment, within the limits of the analysis accuracy.

The Rh/CeO_2 sample behavior was quite different from that of ceria samples for the reduction process (Figure 6C). Reduction was achieved within the collection time of one spectrum (12 s), whatever the temperature, in the range 573–773 K. We failed to detect an intermediate behavior by decreasing the recording time to 4 s. This means that the initial reduction rate was much faster than the recording time of the spectrum, i.e. 4 s. The extent of reduction was 23% ± 2%, whatever the reduction temperature. This value remained unchanged even after 3 h under hydrogen flow. We noted also that we could not fit the initial XAS spectrum, before introducing the hydrogen, with the three lines characteristic of the Ce(IV) state only. We had to introduce a small but definite contribution B_0, characteristic of the Ce(III) line, which represented about 3–5% of the total area of the edge.

In order to fit these data, we have developed a kinetic model for ceria reduction. This model is depicted in Scheme 1 and

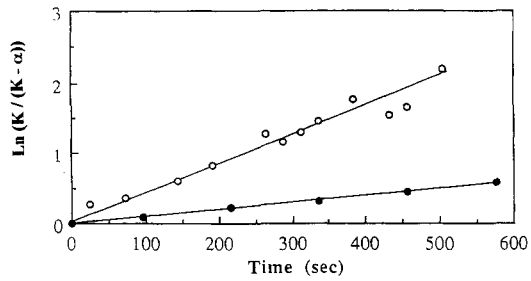

Figure 8. Plot of $\ln(K/K-\alpha(t)) = f(t)$: CeO_2 sample A_1 at 593 K (filled circles) and 673 K (empty circles); full line, fit according to eq 18; time scale 0–600 s. The experimental values of K are reported in Table 4.

SCHEME 1

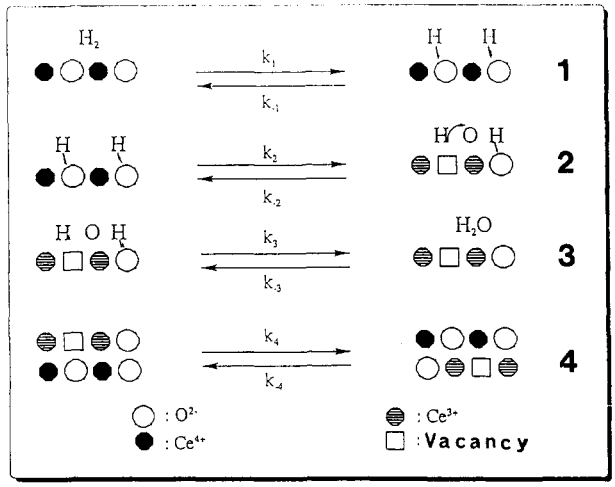

TABLE 3: Parameters of the Reduction Conversion $\alpha = f(t)$ Deduced from Eqs 7–15

rate-limiting step	k	$\alpha(t = 0)$
1	$k_1P_{H2O}/4K_1K_2K_3$	0
2	$k_2P_{H2O}/2SK_2K_3(K_1P_{H2})^{1/2}$	0
3	$k_3P_{H2O}/4K_3$	$A_s^*(T)$
4	$k_4/K_4(1-N_s)$	$A_s^*(T)$

detailed in the Appendix. In this classical model of heterogeneous gas–solid reduction,[35] we explicitly took into account both surface and bulk steps. Surface steps include successively (1) dissociative chemisorption of hydrogen onto the surface to form hydroxyl groups (step 1), (2) anionic vacancy formation with reduction of the neighboring cations (step 2), and (3) water desorption (step 3).

Following these steps, diffusion of the surface anionic vacancies into the bulk occurs (step 4).

With pure ceria, the results strongly suggested that one of the surface steps was rate limiting. We linked then the reduction of a surface layer to the surface area of the sample. We showed that the reduction conversion $\alpha(t)$ can be expressed by the following differential equation:

$$d\alpha/(\alpha - K) = -k\,dt \qquad (4)$$

where k is the rate constant of the process and K a constant depending both on the thermodynamic equilibrium of the surface steps and on a partition function between surface and bulk sites. The expressions of the constants k and K depend on the rate-determining step. The K expression is reported in the Appendix (eq 16). The k expressions depend on the rate-limiting step. They are displayed in Table 3.

Whatever the rate-limiting step, we obtained by integrating eq 4 a straight line in the proper $\ln(K/K-\alpha(t)) = f(t)$ representation. The experimental data fitted such a representation for pure ceria (Figure 8). The experimental values of the parameters K and k

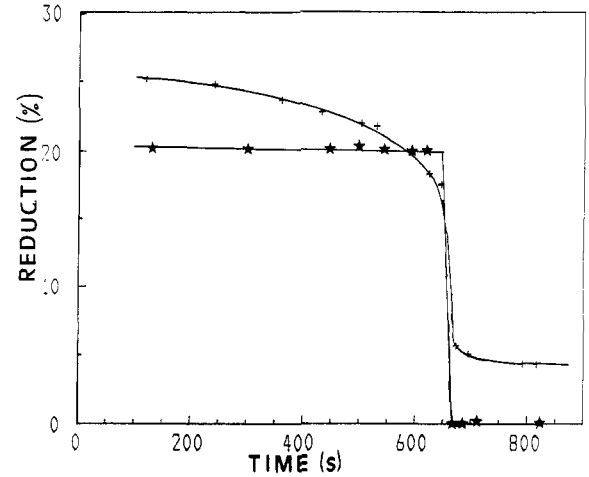

Figure 9. Kinetics of reoxidation measured from the Ce L_{III} edge evolution as a function of time. The curves are scaled to the inflexion point of the reoxidation process: star, CeO_2 A_1 at 673 K; cross, Rh/CeO_2 at 673 K.

TABLE 4: Kinetic Parameters Used in the Modeling of the Surface Reduction (Empty Circles of Figure 10) and the Diffusion (Filled Circles of Figure 10) Steps at Various Temperatures

		surface reduction			diffusion			
sample	T (K)	rate-limiting step	K (%)	k (10^{-3} s^{-1})	rate-limiting step	K (%)	$A_s(T)$	k (10^{-5} s^{-1})
A_1	593	1 or 2	6	0.82	4	40	6	0.5
A_1	633	1 or 2	8	2.1	4	40	8	1.0
A_1	673	1 or 2	20	3.4	4	40	20	1.3
B	673	3 or 4	23	≥80				

are reported in Table 4. The k values were deduced from these fits. They were in good agreement with those determined by the slope of the initial reduction versus time (Figure 6). The K values were adjustable thermodynamic parameters which were estimated from the degree of reduction at the end of the surface process.

In contrast, the large initial reduction rate observed on the Rh/CeO_2 sample precluded the determination of any kinetic parameter. According to the model however, the occurrence of an initial reduction strongly suggested that either step 3 (water desorption) or step 4 (bulk diffusion) was rate limiting.

(b) Reoxidation. The kinetics of reoxidation are plotted in Figure 9. CeO_2 and Rh/CeO_2 samples exhibited quite different behavior. On CeO_2 sample A_1, the reoxidation occurred at so high a rate that the process was completely achieved within the time acquisition of one spectrum. Attempts to detect an intermediate state of CeO_2, by decreasing the recording time down to 2 s but at the expense of the signal to noise ratio, were unsuccessful.

On Rh/CeO_2 however, the process was fast but needs some induction time. We checked that this induction time was dependent on air flow, an effect that did not exist at all on pure ceria. Moreover, as noted for the reduction process, the reoxidation process was not complete. About 3-5% of the cerium remained at the III state even after a long reoxidation time.

Let us conclude finally on a general remark: the CeO_2 and Rh/CeO_2 samples behaved inversely. The reduction kinetics was quite fast on Rh/CeO_2 and slower on CeO_2. The inverse was observed in the reoxidation process.

(3) N_2O Reactivity. N_2O adsorption measurements were performed on the CeO_2 sample A_1 in the temperature range 573–673 K. The aim was then to monitor the reduction kinetics on a larger time scale than that of the XAS experiment (up to 1500 min compared to 120 min). The results concerning the evolution at 673 K are presented in Figure 6A. The agreement between the two measurements is satisfactory. A similar behavior was observed in the range 573–673 K. The difference between the

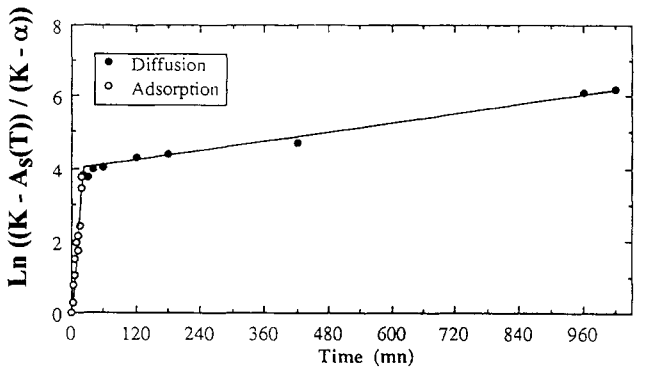

Figure 10. Plot of $\ln((K-A_s(T))/(K-\alpha)) = f(t)$: CeO_2 sample A_1 at 673 K; time scale 0–1000 min. Experimental points are extracted from XAS analysis or N_2O adsorption: empty circles, step 1 or 2 as the rate-limiting step; filled circles, bulk diffusion as the rate-limiting step; solid line, reduction rate deduced from eq 18. The values of the k and K parameters extracted from these fits are reported in Table 4.

two sets of data at a given reduction time never exceeds 3%, the N_2O chemisorption value being generally slightly lower than that extracted from the Ce L_{III} edge analysis.

A reduction process monitored over a large time scale pointed out that the ceria sample A_1 did not reach an equilibrium, even after more than 1000 min of H_2 exposure. Attempts to fit the set of both XAS and N_2O adsorption data within a first-order $\ln(K/(K-\alpha(t))) = f(t)$ kinetic representation, as in Figure 8, were unsuccessful. Moreover, we detected an inflexion point whose value was increasing with the reduction temperature. At 673 K, this inflexion point reached about 20%. According to the model developed in the Appendix, we believed that this inflexion corresponded to a transition from a surface process to a bulk process. We assumed then that the overall kinetic process involved two successive processes, with highly different reaction rates. The fast first step was a surface reaction (step 1 or 2), followed by slow diffusion into the bulk (step 4). The proper representation was then $\ln((K-A_s(T))/(K-\alpha(t))) = f(t)$, where $A_s(T)$ is the surface reduction at the beginning of the bulk diffusion. For example, we quoted $A_s(T) = 0.2$, by extrapolating to zero time the bulk diffusion part of the curve. For sample A_1 at 673 K, this value of $A_s(T)$ agrees well with the calculated value A_s^∞ of the complete reduction of a surface monolayer.[36] A_s^∞ is calculated according to eq 21 in the Appendix. As shown in Figure 10, experimental data nicely fitted this representation. We considered therefore that this model can be an acceptable description of the kinetic process of reduction. Useful information can then be extracted from the parameters k, K, and $A_s(T)$ deduced from these fits. They are reported in Table 4.

(1) The surface reduction at the end of the surface process $A_s(T)$ widely increased in the temperature range 573–673 K. The surface reduction at 673 K corresponded to the upper limit of A_s^∞, where the whole ceria surface was reduced.

(2) Comparing the slopes of the bulk and the surface processes, we concluded that the rate constant was about 2 orders of magnitude lower in the bulk process.

(3) We determined an activation energy of about 21 kJ/mol for the diffusion step 4 in the temperature range 573–673 K.

V. Discussion

Before discussing the kinetic results concerning ceria, let us first consider the usefulness of X-ray absorption experiments compared to other probes. The goal of this paper was to extract the reduction content of ceria after a short reduction time from shape modifications of the Ce L_{III} edge. Below 673 K the ceria surface is stable under hydrogen, and a comparison with TGA, N_2O adsorption, and magnetic susceptibility measurements results can proceed on the same sample, A1, and with a comparable reduction time. At 673 K the degree of reduction after 2 h of reduction are quoted as 24% (XAS) and 26% (N_2O adsorption), which compares favorably with the value of 22% reported by magnetic measurements.[12] After 20 h of reduction, the degree of reduction is respectively 32% (TGA), 36% (N_2O adsorption), and 32% (magnetic susceptibility[12]), respectively. We note that after only 20 min of reduction, the reduction reported by XAS was already 20%. Fast surface reduction is also pointed out by XPS modifications of the Ce 3d core level.[17,33] These comparisons point out (1) the good agreement between the determination of the reduction conversion by different probes and (2) the clear occurrence of a slow reduction that follows the fast reduction process achieved in about 20 min.

This agreement is achieved in spite of the complexity of the Ce L_{III} edge when the Ce(IV) oxidation state is involved. This reliability allows us to specify safely the relative energy position of the many Ce(IV) features (B_1, B_2, and C) between them and relative to the Ce(III) feature B_0 (Table 2). For example, we report an energy separation of 1.85 eV between the B_0 and B_1 contributions and 3.8 eV between the B_1 and B_2 contributions. Up to now, the relative energy positions of the Ce(IV) features were only partially reported.[25,27] Let us recall however that the energy position of these contributions can slightly shift when the anion environment around cerium cations or the nature of the rare earth cation changes. Energy shifts are reported on chemically mixed CeO_2–TiO_2 oxides[32] and on rare earth oxides of the similar fluorite structure (PrO_2, TbO_2).[25]

Let us now consider the change in cerium oxidation state induced by reduction and oxidation processes, respectively.

A. Reduction. TGA, XAS, and N_2O adsorption emphasize *the influence of the specific surface area and the presence of a transition metal* on the reduction kinetics of ceria.

(1) Influence of the Specific Surface Area. The effect of the surface area is clearly pointed out by the different reduction behavior of samples A_1 and A_2 (or A_3). These samples differ only by their surface area, high and low for A_1 and A_2, respectively. More precisely, the model that we developed in the Appendix points out that on pure ceria (i) the first step of the process is a surface step and (ii) a correlation can be found between the optimum extent of reduction of this first step and the amount of anionic surface sites.

As a consequence of these two points, the reduction extent in a short time range is highly sensitive to the surface area. It is only when much of the surface sites are reduced that bulk reduction begins to occur, in the temperature domain considered here.

The first point (i) is ascertained by an initial reduction of ceria from 0 to around 20%. At this value, a break in the kinetics occurs and further reduction is much more slower. The first part of the kinetics agrees well with a model where a surface step is rate limiting (see Appendix). These surface steps involve hydrogen dissociation (step 1) and anion vacancies formation with cation reduction (step 2), respectively (Scheme 1).

An alternative pathway to a surface reaction is invoked by Fierro et al.[10] and Cunningham et al.[34] They invoke the formation of a bronze CeO_2H_x followed by a bulk reduction, according to reactions V and VI:

$$CeO_2 + (x/2)H_2 \rightarrow CeO_2H_x \qquad \text{(V)}$$

$$CeO_2H_x \rightarrow (x/2)H_2O + CeO_{(2-x)} \qquad \text{(VI)}$$

We failed to observe the TGA any weight gain above 393 K. We believe this observation does not mean that any bronze formation did not take place, but the high surface area of sample A_1 enhances the surface process to the detriment of a bulk process.

Anyway, a reduction process according to a bronze formation can be ruled out for the following reasons:

(1) This bronze is reported to be unstable at temperatures higher than 573 K.

(2) A bronze formation and a bulk reduction, according to eqs V and VI, cannot explain the break in the reduction kinetics at about 20–23% of sample A_1 at 673 K.

(3) Such a process supposes a high rate of bulk water diffusion through preferential pathways like grain boundaries diffusion. This seems unlikely.

As far as the second point (ii) is concerned, we can roughly evaluate the proportion of surface anionic sites in the function of the surface area. This evaluation had been developed by Johnson and Mooi.[36] The expressions are reported in the Appendix. The proportion of surface anionic sites N_s^A is then given by eq 19. The complete reduction of a surface monolayer A_s^∞ is given by eq 21, assuming that the creation of a surface oxygen vacancy results in the reduction of two adjacent Ce(IV) ions into Ce(III) ions. We calculate then a reduction content of 3 and 22% for surface areas of 8 and 120 m^2/g corresponding to the samples A_1 and A_2, respectively. These results compare favorably with the experimental values of 4 and 23% obtained after 20 min of reduction at 673 K for samples A_1 and A_2, respectively. This is just before the break of the slope in the $\ln((K\text{-}A_s(T))/(K\text{-}\alpha(t))) = f(t)$ representation. We believe an even more accurate determination of the surface reduction is provided by considering the break in the kinetic behavior of ceria reduction (Figure 10). We assign this change of slope to the slow bulk diffusion of anion vacancies that follows the fast surface reduction. An extrapolation to zero time gives then a value of 20% for sample A_1.

The occurrence of reduction for ceria must be discussed however from a thermodynamic point of view. Ceria is well-known to be difficult to reduce, especially in the temperature range 573–773 K. Then at given temperature and partial pressure ratio P_{H2}/P_{H2O}, to what extent is ceria reduction afforded? We can estimate it by determining the equilibrium constant K_p of the overall equilibrium VII:

$$2CeO_2 + H_2 \rightarrow Ce_2O_3 + H_2O \qquad \text{(VII)}$$

The free enthalpies of Ce_2O_3 and CeO_2 formation are given respectively by eqs 5 and 6:[37]

$$\Delta G_f^\circ(Ce_2O_3) = -424100 + 65.8T \text{ (cal/mol)} \qquad (5)$$

$$\Delta G_f^\circ(CeO_2) = -259650 + 50.7T \text{ (cal/mol)} \qquad (6)$$

whereas the oxygen partial pressure is determined from equilibrium VIII:[38]

$$H_2 + {}^1/_2O_2 \rightarrow H_2O(g) \qquad \text{(VIII)}$$

Unfortunately, the real partial pressure ratio P_{H2}/P_{H2O} above the surface is unknown. We only know the initial partial pressure ratio, which is lower than 10^{-5}. Using the data of eqs 5 and 6, we can estimate that reduction readily occurs only if the water pressure above the surface does not exceed about 10^{-4} atm. We must recall however that these simple considerations neglect possible thermodynamic stabilization in one of the numerous substoichiometric oxides.[39-42] We can nevertheless state that reduction is thermodynamically possible, provided that the water partial pressure above the surface of the sample does not exceed too far the residual water pressure in the gas phase.

Reduction of ceria has been already studied in the literature, but comparison with other kinetic data is rather limited as the partial pressure ratio P_{H2}/P_{H2O} and the contact time are widely changed and often not accurately controlled, according to the used probe and experimental conditions. Yao et al.[3] reported by thermoprogrammed reduction a negligible reduction at 673 K, but on ceria samples of very low surface area. Otsuka et al.[9] reported cycles of reduction–reoxidation at temperatures above 873 K. They noted a decrease of the surface area during the cycle. This means that the surface of these samples was probably not stabilized. Fierro et al.[10] noted a reduction of about 0.11 at 653 K for a ceria of surface area 58.7 m^2/g, a value in good agreement with a fully reduced surface, if we consider the relationship of Johnson and Mooi[36] (eqs 20 and 21). Laachir et al.[12] monitored the reduction of the same samples, A_1 and A_2, by magnetic susceptibility measurements, TPR, XPS, FTIR, and UV–visible reflectance spectroscopy. They reported a reduction content of 21% after 120 min on sample A_1 and a negligible reduction content on sample A_2 at 673 K, in excellent agreement with our data. They also point out that the reduction is still occurring up to 20 h. They then obtained a reduction of 32%. This comparison with literature thus strongly suggests that ceria reduction at moderate temperature is initially governed by a surface reduction process.

We observe however that the reduction extent on sample A_1 sharply decreases above 673 K. Moreover, the kinetic curves are then rather disturbed. We believe this can be correlated with the sharp decrease in the surface area observed on this sample under hydrogen above 673 K.[16] Assuming that the bulk reduction remains negligible, we suggest therefore that two effects are then competing in opposite senses: (i) a physical process of pore filling resulting in a loss of surface site density and (ii) the chemical reduction of these surface sites. The apparent decrease of the degree of reduction suggests that the pore-filling process is less activated.

In the framework of our model, it is helpful to address the question of the rate-determining step among the three surface steps. This is possible as, even if bulk reduction is obviously the limiting step of the overall process, the surface rate is so low that it may be considered independent of the bulk reduction.

Considering the initial rate of reduction, we report an apparent activation energy of 67 kJ/mol. As we cannot settle which step, 1, 2, or 3, is the rate-determining step of the surface reaction, a comparison of the activation energy with data from the literature can be of useful help. Data can be extracted for activation energies of ceria reduction including H_2 or CO as reductive reagent,[8-10,43-46] oxygen self-diffusion,[47] and ionic conductivity.[48,49] Other data concerning praseodymia and terbia of similar structure are also available.[37] We must here keep in mind two factors when comparing our results with these data. First, the activation energies depend on the oxygen partial pressure, P_{O2}.[47] As stated above, P_{O2} over the surface is unknown, but an upper limit of P_{H2O}/P_{H2} quoted to 10^{-4} atm can be estimated. Second, one must take into consideration the high density of surface sites of sample A_1. Then activation energies can be strongly modified through lateral interactions between the surface sites. Despite these two limitations, useful information can be extracted from the literature. We can thus clearly rule out a phase boundary process of reduction as both (i) the kinetic law does not obey such a process and (ii) the activation energy is much higher (about 210 kJ/mol).[37] Activation energies of 155 kJ/mol[9] and 138 kJ/mol[10] were reported for ceria reduction of low or medium surface areas by H_2. These authors concluded that hydrogen dissociation was the rate-limiting step. Guenin[45] and Breysse et al.,[8] in an accurate study of ceria reduction by CO, determined an activation energy of 84 kJ/mol for the formation of an oxygen vacancy. This can be compared also with the activation energy of oxygen self-diffusion through a vacancy mechanism (100 kJ/mol).[47] However the oxygen self-diffusion process is reported to vary from 100 to 17 kJ/mol in $CeO_{(2-x)}$ when x increases from 0 to 0.18.[47] Similarly, activation energies of ionic conductivity are reported to vary from 105 kJ/mol for $x = 0.01$ to 71 kJ/mol for $x = 0.2$, respectively.[49] The lack of information on the real P_{O2} pressure, the possible occurrence of lateral interactions at high surface area, and the wide variation of the activation energy of oxygen vacancy formation with the content of oxygen vacancy complicate any comparison with literature. However, owing to

the results obtained with the presence of rhodium that we shall discuss later, we believe that step 1 of dissociative hydrogen adsorption is limitative of the surface reduction. As a matter of fact, the main effect of rhodium is to hugely increase this rate of hydrogen dissociation.

A bulk diffusion process follows the initial surface step. We determine an activation energy of 21 kJ/mol for this step. This value compares favorably with literature data for a bulk diffusion through a vacancy mechanism.[50] We must keep in mind however that the activation energies for oxygen self-diffusion or ionic conductivity are also strongly dependent on the vacancy content and the crystallographic structure of the substoichiometric oxide.

(2) Influence of the Transition Metal. The addition of rhodium modifies strongly the reduction kinetics. The reduction amounts instantaneously to 23–25%, close to the complete surface reduction. We estimate then that the initial reduction rate constant at 673 K exceeds 0.08 s^{-1}. According to our model, this immediate reduction of part of the ceria implies that the surface steps 1 and 2 becomes very fast. Then either step 3 or 4 is rate determining. Step 3 involves water desorption from the surface, and step 4 is the diffusion of the anionic vacancies into the bulk of the solid. Several reasons lead us however to rule out a slow water desorption step 3:

(1) Water evolution on Rh/CeO_2 occurs at much lower temperatures, as detected by thermoprogrammed desorption.[51]

(2) A high water partial pressure above the surface will inhibit ceria reduction.

The high rate of the initial surface reduction can be explained by the well-known hydrogen dissociation on metallic rhodium, as on other transition metal such as Pt, Pd, etc. This hydrogen, probably in a very reactive form, can then spill over the support where it allows the removal of surface oxygen and create a surface vacancy. The initial reduction on Rh/CeO_2 is ca. 22–24%, a value close to the value of the fully reduced surface deduced from the extrapolation to zero time on a pure ceria sample or to the value calculated according to eq 21. This means that the whole surface is immediately reduced. This is in good agreement with XPS investigations on the same samples.[33] Furthermore, as discussed later, this reduced surface is not completely removed upon further reoxidation.

After this fast surface reduction step, we fail to detect further noticeable reduction. TGA provides additional information on this point: the deficit in weight loss between the Rh/CeO_2 and the CeO_2 samples can be explained by a lower extent of the overall ceria reduction in the presence of rhodium. Assuming a full reduction of the metal and the complete surface reduction of ceria, this means that the presence of a transition metal inhibits the oxygen vacancy diffusion inside the bulk of ceria. This can be understood within the model of oxygen vacancy filling by transition metal atoms[56] that blocks the diffusion. The atomic radius of rhodium (0.134 nm) compares fairly well with the oxygen ionic radius in ceria (0.1356 nm).[37]

We conclude then that, compared to the pure ceria, the reduction process in the presence of rhodium is much faster but, on a larger time scale, the extent of this reduction is lower.

B. Reoxidation. By comparison with reduction, the kinetics of reoxidation is far simpler on pure ceria. The reoxidation rate is much faster than the time scale needed to record the Ce L_{III} absorption edge. We can thus estimate it to exceed 0.08 s^{-1}. This is in agreement with the literature data, where anomalously high rates of reoxidation were reported, even at room temperature.[52] Furthermore, the reoxidation is complete.

By contrast, the reoxidation of cerium in Rh/CeO_2 needs an induction time before starting up and is not complete. These two points deserve a discussion.

We note that we still measure an irreversible content of Ce(III) cations with the presence of rhodium under air at 673 K. The content of these Ce(III) cations amounts to 3–5%, which is within experimental error. It could be explained by an energy shift of the absorption contribution B_0 due to the presence of rhodium in interaction with ceria. We cannot also exclude the possibility of an irreversible and partial reduction of the ceria support (surface and/or bulk) by a strong interaction with the transition metal. More probably, a chemical effect by formation of a cerium chloride or oxychloride can be invoked. These species can easily be obtained by reaction of the rhodium chloride, $RhCl_3$, precursor with the rare earth oxide. The cerium oxidation state in such compounds is III. Similar species have been identified on palladium and cerium or other rare earth catalysts.[5,13] The cerium oxychloride is stable under an air atmosphere up to 723 K and is decomposed above this temperature.[53] Assuming the quantitative formation of the oxychloride, we calculate a Ce(III) content of 6%, on the basis of the remaining chlorine content at 673 K reported in Table 1. This value is not far from the experimental one of 3–5% for the irreversible content of Ce(III) cations.

Otherwise, the occurrence of an induction time is supported by a recent similar study on a $Pt/Rh/CeO_2/Al_2O_3$ depollution catalyst[54] and by thermoprogrammed oxidations which point out oxygen consumptions at high temperature on Pd/CeO_2 catalysts.[55] Tentative explanations must taken into account the presence of the transition metal. Recent EXAFS investigations on a $Pt/Rh/Ce/Al_2O_3$ catalyst outline the occupation by metallic atoms of oxygen vacancy sites.[54] Again, we can invoke the Sanchez and Gasquez model of oxygen vacancy filling by transition metal atoms.[56] In the reduced state, metallic atoms are buried into the anionic array of the fluorite crystal. We can therefore suppose that the gaseous oxygen needs first to expel the rhodium atoms from their anionic sites before filling them and then reoxidizing the nearest cerium atoms. The first step of the process is then believed to be the oxidation of the metallic rhodium buried in the ceria anionic array, a process which is supposed to be much slower than the ceria reoxidation itself. We must also note that the surface anionic sites N_s^A on sample A_1 calculated according to eq 19 are in large excess compared to rhodium atoms.

Alternative explanations involve a strong electronic interaction between rhodium and the first surface layers of ceria which prevents the fast reoxidation of the support. In a similar way we can suppose the formation of a surface phase of rhodium and some layers of reduced ceria in a different crystallographic rearrangement. Thus, for the very rich phase diagram of ceria at temperatures below 707 K, the phase transition of the ordered substoichiometric phase labeled δ to the phase labeled α requires a crystallographic rearrangement, which is an activated process.[42] Whatever the explanation, complementary works require the acquisition of structural information of these samples under controlled gas conditions. EXAFS experiments, which can be carried out in similar conditions, seem to be adapted to answer this problem.

Finally, these results could be related to the properties of ceria in the depollution catalysis. Ceria is well-known to be able to store oxygen in the course of the depollution process. In spite of the widely different temperature range and gas environment between our study and the depollution process, the observation that in the presence of rhodium the rate of oxidation slows down whereas the rate of reduction dramatically accelerates can support an explanation on the behavior of ceria in depollution catalysis. As these two reactions have then comparable rates, ceria can store and remove oxygen in the very short time of the depollution process, working in non-steady-state conditions. In contrast, pure ceria cannot possess the same behavior, as the oxidation rate is much faster than the reduction rate. Further works, including the proper temperature range and gas environment and time scale studies, are needed however to check these considerations.

VI. Conclusions

The main results of this work are summarized as follows:

(1) XAS measurements recorded in the fast acquisition mode prove to be an efficient probe to monitor the change in cerium oxidation state within a short kinetic process.

(2) Combined use of XAS with TGA and N_2O adsorption allows us to describe the kinetic behavior of ceria or ceria-based systems modified by a transition metal on a large time scale. The XAS probe is however of limited use for very fast processes such as those with a first-order rate constant larger than 0.1 s^{-1}.

(3) The reduction content of pure ceria is highly dependent on the surface area. The reduction occurs preliminarily through a surface process.

(4) The redox behavior of Rh/CeO_2 is quite different from that of pure ceria. In the presence of a transition metal, the reduction rate is highly increased, whereas the oxidation rate needs an induction time before starting.

(5) A kinetic model of ceria reduction is developed that takes into account the two effects of the surface area and the presence of a transition metal. Ceria reduction occurs first through a surface limitative step, probably hydrogen dissociation, followed by a much slower bulk diffusion step. The rate of the surface step is highly increased on Rh/CeO_2 samples through fast hydrogen dissociation on rhodium.

Acknowledgment. This work has been supported by the Ministère de la Recherche under the project MRES No. 87 0566 "Nouveaux Matériaux Catalytiques à base de Terres Rares". The contribution of the LURE staff (P. Lagarde, C. Prieto) to the success of the absorption experiments has been greatly appreciated.

Appendix

Modeling of the Reduction Kinetics of Ceria with a Large Surface Area. The reduction of ceria can be described according to a four-step process displayed in Scheme 1. This is a general scheme for heterogeneous gas–solid reduction.[35] We add further relations taking into account the large surface area of the sample A_1.

1. Dissociative adsorption of dihydrogen. Gaseous dihydrogen is dissociatively adsorbed on the surface to form hydroxyl groups. We assume that (i) the surface is formed by an alternate array of anionic and cationic sites.[110] The (110) surface is a dense surface of this kind for a CaF_2 cubic lattice like CeO_2. Observations by electron microscopy suggest that they are the most prominent on sample A1.[16] (ii) The stoichiometry of adsorption is one atomic hydrogen for one anion site. (iii) The hydrogen dissociation occurs exclusively on Ce^{4+} sites. (iv) Adsorbed molecular water is negligible at the high reaction temperature where the kinetics was carried out, and (v) lateral interactions between adjacent sites are neglected. FTIR investigations carried out on samples A1 and A2 provide us justification for some of these assumptions.[12] The absence of any ν(OH) band characteristic of adsorbed water above 673 K strongly supports point iv. Points ii and iii can be justified by the main occurrence of ν(OH) bands of bidentate species adsorbed on Ce(IV) cations at T values below 573 K and on Ce(III) cations above 573 K.

The kinetic rate of hydrogen dissociation, V_1, can then be written as

$$V_1 = (k_1(1 - \theta_H - \theta_{OH})^2 P_{H2}) - (k_{-1}\theta^2{}_H) \qquad (7)$$

where θ_H and θ_{OH} represent the atomic hydrogen and hydroxyl group surface coverages, respectively; in this equation and further eqs 8 and 10, k_i and k_{-i} (i = 1, 2, 3) are direct and inverse first-order kinetic constants of the step i of the reduction process, respectively. P_{H2} is the partial pressure of hydrogen.

2. Formation of Anionic Vacancies with Cation Reduction. The adsorbed hydrogen contributes to the reduction of the cation from Ce(IV) to Ce(III) by formation of an anionic vacancy. The rate, V_2, of this step can be expressed as follows:

$$V_2 = (2k_2\theta_H) - (2k_{-2}C_s{}^A\theta_{OH}) \qquad (8)$$

where $C_S{}^A$ represents the surface concentration in anionic vacancies. Here the factor 2 takes into account the probability of oxygen vacancy formation relative to the dissociation of one hydrogen molecule. We introduce then the surface concentration in reduced cations α_S. Assuming that the creation of an oxygen vacancy results in the reduction of two adjacent Ce(IV) cations, we derive the following relationship:

$$2C_s{}^A = \alpha_s \qquad (9)$$

3. Water Desorption. Water is desorbed from the surface by the recombination of hydrogen and a hydroxyl group. The rate of this water formation step, V_3, is then

$$V_3 = (k_3 C_s{}^A \theta_{OH}\theta_H) - (k_{-3}(1 - \theta_H - \theta_{OH})C_s{}^A P_{H2O}) \qquad (10)$$

where P_{H2O} is the water partial pressure.

4. Bulk Diffusion. The surface anionic vacancies diffuse inside the bulk of the solid according to step 4 of the scheme. The rate of this step can be expressed as

$$V_4 = 2k_4\alpha_s - 2k_{-4}\alpha_b \qquad (11)$$

where k_4 and k_{-4} are diffusion constants, from the surface to the bulk and the bulk to the surface, respectively. α_b is the bulk concentration of reduced cationic sites. We assume therefore that the anionic vacancies are randomly distributed onto the surface, without any ordering in their distribution. This implies thus that diffusion occurs without preferential ways. Although reduced cerium dioxide is well-known to be able to order anionic vacancies,[39] we can justify this assumption by the low reductions ($\alpha \leq 20\%$) that we obtain with our experimental conditions.

Finally, we introduce the overall reduction α defined as the overall concentration (bulk and surface) of the reduced cations. α is a linear combination of the surface α_s and the bulk α_b concentration of reduced cations according to

$$\alpha = (\alpha_s N_s{}^C) + (\alpha_b N_b{}^C) \qquad (12)$$

$$N_s{}^C + N_b{}^C = 1 \qquad (13)$$

where $N_s{}^C$ and $N_b{}^C$ are the relative content of surface and bulk cationic sites, respectively. For a solid of low surface area, $N_s{}^C \ll N_b{}^C \approx 1$ and $\alpha \approx \alpha_b$, but for a solid of high specific area such as the sample A_1, $N_s{}^C$ becomes non-negligible compared to $N_b{}^C$.

To resolve the kinetic system represented by eqs 7–13, we must introduce an assumption concerning the rate-limiting step. Whatever the step i, we suppose that the rate of reduction can be expressed as

$$2(d\alpha/dt) = V_i \qquad (14)$$

$$V_j = 0 \quad (j \neq i) \qquad (15)$$

The resolution of this system is analytically possible only if the free anionic site coverage ($1 - \theta_H - \theta_{OH}$) largely exceeds the hydrogen and hydroxyl coverages. This assumption can be justified by the report that the H_2O and H_2 contents desorbed by TPR on sample A1 are low.[12] The resolution of the system

represented by eqs 7–13 then leads to the differential eq 4:

$$d\alpha/(\alpha - K) = -k\,dt \quad (4)$$

where

$$K = 2S(\Pi_i^{(i=1-3)}K_i)(P_{H2}/P_{H2O}) \quad (16)$$

and

$$S = N_s^C + K_4(1 - N_s^C) \quad (17)$$

K is a thermodynamic equilibrium constant at the given ratio of partial pressures (P_{H2}/P_{H2O}) weighted by a partition factor S. This partition factor given by eq 17 accounts for the probability distribution of the reduced cations between surface and bulk sites.

In the differential eq 4 the rate constant k and the initial reduction at $t = 0$ differ according to the rate-limiting step i (Table 3). As we have no prerequisite idea on it, we have developed the rate-limiting-step condition for the four possible steps of the reduction process. An integration of the differential eq 4 leads to an expression of the form

$$\ln((K - \alpha(t=0))/(K - \alpha(t))) = kt \quad (18)$$

The calculated rate constants k and initial reduction $\alpha_{(t=0)}$ are reported in Table 3. The initial reduction is quoted to 0 (step 1 or 2) or $A_s(T)$ (step 3 or 4), the surface reduction at the temperature T, according to the rate-limiting step.

Finally, several remarks can be made on the kinetic expressions of the reduction rate $\alpha(t)$.

(1) The expressions obtained by considering steps 1 and 2 or steps 3 and 4 are exactly similar, except the initial reduction. We cannot distinguish then by this model which of the steps 1 or 2 or steps 3 and 4 are limitative. Only experiments as a function of the partial pressures P_{H2} and P_{H2O} allow a clear discrimination between them.

(2) The reduction on pure ceria and 1.45 Rh/CeO_2 samples was fitted according to this model. In the case of pure ceria, we can distinguish two domains with a break point. Within these two domains we fit independently the kinetic curves. This is possible as the rate of surface reduction is much larger than that of the bulk reduction. The parameters of these fits are reported in Table 4. An example of fit is reported in Figure 10. We note that the equilibrium constant K increases with the temperature and that the K values obtained at 673 K for CeO_2 and Rh/CeO_2 are close.

(3) The value of $A_s(T)$ at 673 K agrees well with a complete reduction of the surface (0.20 instead of 0.23, respectively). At lower temperatures, $A_s(T)$ is much lower. This indicates that the surface reduction is not completely achieved below 673 K.

Finally, we need to estimate A_s^∞. This value provides an upper limit of the surface reduction process. This was performed by calculating the proportion of surface anionic sites as a function of the surface area. The number of surface anionic sites N_s^A has been calculated by Johnson and Mooi[36] as a function of the number n of anionic sites O^{2-} located on the edge of a ceria particle of cubic form:

$$N_s^A = (6n^2 - 12n + 8)/n^3 \quad (19)$$

We assume that $N_s^A = 2N_s^C$, both on the surface and inside the particle. If the ceria particle develops a surface area S_{BET}, n can be expressed as

$$n = F/(adS_{BET}) \quad (20)$$

where F is a geometrical factor taking into account the number of faces exposed to the gas environment ($F = 6$ for a cube), a is the diameter of the oxygen ion (0.28 nm), and d is the density of the material (7.13 g/cm^3).

From eqs 9 and 19, we can derivate the complete reduction of a surface layer A_s^∞, which is a close function of the surface area, according to eq 20:

$$A_s^\infty = 2(6n^2 - 12n + 8)/n^3 = f(S_{BET}) \quad (21)$$

A_s^∞ values of 5% and 22% are calculated according to eq 16 for samples A_1 and A_2 of surface areas 125 and 8 m^2/g, respectively.

References and Notes

(1) Taylor, K. C. In *Catalysis, Science and Technology*; Anderson, J. R., Boudart, M., Eds.; Springer Verlag: Berlin, 1984; Vol. 5, p 119.
(2) Yao, Y. F. Y. *J. Catal.* **1984**, *87*, 152.
(3) Yao, F. C.; Yao, Y. F. Y. *J. Catal.* **1984**, *86*, 256.
(4) Jin, T.; Zhou, Y.; Mains, J.; White, J. M. *J. Phys. Chem.* **1987**, *91*, 5931.
(5) Le Normand, F.; Hilaire, L.; Kili, K.; Krill, G.; Maire, G. *J. Phys. Chem.* **1988**, *92*, 2561.
(6) Height, T. M.; Bevan, D. J. M. In *Handbook on the Physics and Chemistry of Rare Earths*; Gschneidner, K. A., Jr., Eyring, L., Eds.; North-Holland: Amsterdam, 1979; p 354.
(7) Le Normand, F.; El Fallah, J.; Majerus, J.; Prieto, C.; Touret, O. In *Proceedings of the International Congress on X-Ray Absorption Fine Structure*; Hasnain, S. S., et al., Eds.; Ellis and Herwood Ltd.: Chichester, 1991; Paper 134, p 508.
(8) (a) Breysse, M.; Guenin, M.; Claudel, B.; Veron, J. *J. Catal.* **1973**, *28*, 54. (b) Breysse, M.; Guenin, M.; Claudel, B.; Latreille, H.; Veron, J. *J. Catal.* **1972**, *27*, 275.
(9) (a) Otsuka, K.; Hatano, H.; Morikawa, A. *J. Catal.* **1983**, *79*, 493. (b) Rosynek, M. P. *Catal. Rev. Sci. Eng.* **1977**, *16*, 111. (c) Hattori, T.; Inoko, J. I.; Murakami, Y. *J. Catal.* **1976**, *42*, 60.
(10) Fierro, J. G. L.; Soria, J.; Sanz, J.; Rojo, J. M. *J. Solid State Chem.* **1987**, *66*, 154.
(11) Prieto, C.; Parent, P.; Le Normand, F.; Lagarde, P.; Dexpert, H. In *Proceedings of the 2nd European Conference on the Progress of X-Ray Synchrotron Radiation Research*; Balerna, A., Bernieri, E., Mobilio, S., Eds.; Italian Physics Society: Bologna, 1990; p 411.
(12) Laachir, A.; Perrichon, V.; Badri, A.; Lamotte, J.; Catherine, E.; Lavalley, J. C.; El Fallah, J.; Hilaire, L.; Le Normand, F.; Quéméré, E.; Sauvion, G. N.; Touret, O. *J. Chem. Soc. Faraday Trans. 1* **1991**, *87*, 1601.
(13) Le Normand, F.; Barrault, J.; Breault, R.; Hilaire, L.; Kiennemann, A. *J. Phys. Chem.* **1991**, *95*, 257.
(14) Jin, T.; Okuhara, T.; Mains, J.; White, J. M. *J. Phys. Chem.* **1987**, *91*, 3310.
(15) Briois, V. Thesis, University Pierre et Marie Curie, Paris VI, Sept 1991.
(16) Laachir, A.; Lavalley, J. C.; Martin, G. A.; Perrichon, V.; Touret, O.; Quéméré, E. Unpublished results.
(17) Le Normand, F.; El Fallah, J.; Vasquez, A. To be published.
(18) Lytle, F. W.; Greegor, R. B.; Marques, E. B.; Sandstroem, D. R.; Via, G. H.; Sinfelt, J. H. *J. Catal.* **1985**, *95*, 546.
(19) MacMaster, W. H.; Kerr del Grande, N.; Mallett, J. H.; Hubbell, J. H. In *Compilation of X-Ray Cross Sections*; NTIS (U.S. Dept. of Commerce): 5285 Port Royal Road, Springfield, VA, 22151, Section II, revision 1.
(20) Stern, E. A.; Lu, K. Q. *Nucl. Instrum. Methods* **1983**, *212*, 475.
(21) Dell, R. M.; Stone, F. S.; Tiley, P. F. *J. Chem. Soc. Trans. Faraday Soc.* **1953**, *49*, 195.
(22) (a) Bauchspiess, K. R.; et al. In *Valence Fluctuations in Solids*; Falicov, L. M., Hanke, W., Maple, M. B., Eds.; North-Holland: Amsterdam, 1981; p 417. (b) Beaurepaire, E.; Krill, G.; Le Normand, F. In *4th International Congress of EXAFS and Near Edge Structure*; Lagarde, P., et al., Eds.; Les Editions de Physique: Paris, 1987; p 309.
(23) Bianconi, A.; Marcelli, A.; Tomellini, M.; Davoli, I. *J. Magn. Magn. Mater.* **1985**, *47*, 209.
(24) Kaindl, G.; Wertheim, G. K.; Schmiester, G.; Sampathkumaran, E. V. *Phys. Rev. Lett.* **1987**, *58*, 606.
(25) Dexpert, H.; Karnatak, R. C.; Estéva, J. M.; Connerade, J. P.; Gasgnier, M.; Caro, P. E.; Albert, L. *Phys. Rev. B* **1987**, *36*, 1750.
(26) Kotani, A.; Toyozawa, Y. *J. Phys. Soc. Jpn.* **1973**, *35*, 1073.
(27) Kotani, A.; Jo, T.; Parlebas, J. C. *Adv. Phys.* **1989**, *37*, 37.
(28) Wuilloud, E.; Delley, B.; Schneider, W. D.; Baer, Y. *J. Magn. Magn. Mater.* **1985**, *47*, 197.
(29) Koelling, D. D.; Boring, A. M.; Wood, J. H. *Solid State Commun.* **1983**, *47*, 227.
(30) Angelov, B. M. *J. Phys. Chem.* **1981**, *14*, L757.
(31) Bambynek, W.; Crasemann, B.; Fink, R. W.; Freund, H. U.; Mark, H.; Swift, C. D.; Price, R. E.; Rao, P. V. *Rev. Mod. Phys.* **1972**, *718*.
(32) Dauscher, A.; Hilaire, L.; Le Normand, F.; Muller, W.; Maire, G.; Vasquez, A. *Surf. Int. Anal.* **1990**, *16*, 341.
(33) El Fallah, J. Thesis, University Louis Pasteur, Strasbourg, Jan 1991.
(34) Cunningham, J.; O'Brien, S.; Sanz, J.; Rojo, J. M.; Soria, J. A.; Fierro, J. L. G. *J. Mol. Catal.* **1990**, *57*, 379.
(35) (a) Barret, P., *Cinétique Hétérogène*; Gauthier-Villars: Paris, 1973; p 147. (b) Duffour, L. C.; Perdereau, M. In *Surfaces and Interfaces of Ceramic Materials*; Duffour, L. C., Petot-Ervas, G., Eds.; Kluwer: Amsterdam, 1989; p 419.
(36) Johnson, M. L.; Mooi, J. *J. Catal.* **1987**, *103*, 502.

(37) Eyring, L. In *Handbook on the Physics and Chemistry of Rare Earths*; Gschneidner, K. A., Jr., Eyring, L., Eds.; North-Holland: Amsterdam, 1979; Vol. 3, p 372.
(38) Barrow, G. M. *Physical Chemistry*, 4th ed.; McGraw-Hill: Tokyo, 1979; p 239.
(39) Catlow, C. R. A. In *Non-stoichiometric oxides*; Sorensen, O. T., Ed.; Academic Press: New York, 1981; p 61.
(40) Bevan, B. J. M.; Kordis, J. *J. Inorg. Chem.* **1964**, *26*, 1509.
(41) Brauer, G.; Gingerich, K. A. *J. Inorg. Nucl. Chem.* **1960**, *16*, 87.
(42) Korner, R.; Ricken, M.; Nolting, J.; Riess, I. *J. Solid State Chem.* **1989**, *136*, 16.
(43) Rienacker, G.; Wu, Y. *Z. Anorg. Allg. Chem.* **1962**, *315*, 121.
(44) Hyde, B. G.; Garver, E. E.; Kuntz, U. E.; Eyring, L. *J. Phys. Chem.* **1965**, *69*, 1667.
(45) Guenin, M. *An. Chim.* **1973**, *8*, 147.
(46) Takasu, Y.; Matsui, M.; Tamura, H.; Kawamura, S.; Matsuda, Y.; Toyoshima, I. *J. Catal.* **1981**, *69*, 51.
(47) Steele, P. M.; Floyd, J. M. *Proc. Br. Ceram. Soc.* **1971**, *19*, 55.
(48) Tuller, H. L.; Nowick, A. S. *J. Phys. Chem. Solids* **1977**, *38*, 859.
(49) Wang, D. Y.; Park, D. S.; Griffith, J.; Nowick, A. S. *Solid State Ionics* **1981**, *2*, 95.
(50) Matzke, H. In *Non-stoichiometric oxides*; Sorensen, O. T., Ed.; Academic Press: New York, 1981; p 210.
(51) Laachir, A. Thesis, University Claude Bernard, Lyon, France, 1991.
(52) Ban, Y.; Nowick, A. S. Proc. 5th Mat. Res. Symp., Nation. Bureau of Stand. Spec. Pub.; *Solid State Chem.* **1972**, *364*, 128.
(53) Klevtzov, P. *C. R. Acad. Sci. Ser. C* **1968**, *266*, 385.
(54) Weibel, M.; Garin, F.; Le Normand, F.; Maire, G. To be published.
(55) Le Normand, F.; Barrault, J.; Hilaire, L.; Kili, K. To be published.
(56) Sanchez, M. G.; Gasquez, J. L. *J. Catal.* **1987**, *104*, 120.